VNU Journal of Science: Mathematics - Physics

Journal homepage: https://js.vnu.edu.vn/MaP

Original Article

Hydrothermal Synthesis and Gas Sensing Performance of Spinel-type $SnFe_2O_4$ Nanomaterials: Influence of Synthesis Condition

Tran Thi Viet Nga[1,2,*], Vuong Minh Hieu[1], Nguyen Pham Yen Nhi[2], Nguyen Duc Hoa[2], Chu Manh Hung[1,2]

[1]*International Training Institute for Materials Science Hanoi University of Science and Technology 1 Dai Co Viet, Hanoi, Vietnam*

[2]*School of Materials Science and Engineering, Hanoi University of Science and Technology, 1 Dai Co Viet, Hanoi, Vietnam*

Received 11th August 2025
Revised 10th September 2025; Accepted 30th September 2025

Abstract: In this work, spinel-type $SnFe_2O_4$ nanomaterials were successfully synthesized via hydrothermal method at different temperatures (namely 180 °C, 200 °C, and 220 °C), followed by calcination at 500 °C, to investigate the effects of synthesis conditions on their microstructural characteristics and gas sensing behavior. X-ray diffraction (XRD) analysis confirmed the formation of single-phase spinel $SnFe_2O_4$ with high crystallinity, while SEM images revealed a clear evolution of morphology from irregular agglomerates at 180 °C to uniform spherical nanoparticles at 200 °C, and well-defined cubic structures at 220 °C. Gas sensors made from these nanomaterials exhibited a high sensitivity and stable performance toward the target gases. This demonstrates a potential application of $SnFe_2O_4$ for the sensor fabrication. The results highlight the critical role of hydrothermal temperature in tailoring particle morphology and optimizing the functional properties of $SnFe_2O_4$. These findings suggest that $SnFe_2O_4$ is a promising candidate for next-generation gas sensors, particularly in industrial monitoring and environmental protection.

Keywords: Nanomaterials, Metal oxide, Hydrothermal, Gas sensors, $SnFe_2O_4$.

* Corresponding author.
E-mail address: nga.tranthiviet@hust.edu.vn

https//doi.org/10.25073/2588-1124/vnumap.5059

1. Introduction

Gas sensors are indispensable in diverse applications such as environmental monitoring, industrial process control, and the early detection of toxic or flammable gases [1]. Among various sensing technologies, metal oxide semiconductor (MOS) sensors have gained considerable attention due to their cost-effectiveness, simple fabrication processes, and high sensitivity [2, 3]. Nevertheless, conventional MOS-based sensors suffer from critical drawbacks, including poor selectivity, high operating temperatures, and performance degradation under humid conditions, which hinder their widespread deployment in real-world environments [4, 5].

Recent advances in nanotechnology have enabled the development of nanostructured materials with tailored morphologies and compositions to address these limitations. Ternary metal oxides such as Zn_2SnO_4, $SnFe_2O_4$, and $ZnCo_2O_4$ have emerged as promising candidates for gas sensing applications due to their excellent thermal and chemical stability, abundant redox-active sites, and tunable electronic properties [6, 7]. Within this category, spinel-type metal oxides, particularly ferrites with the general formula MFe_2O_4 or MCo_2O_4 (where M is a divalent metal ion), offer attractive features such as structural robustness, modifiable electronic behavior, and enhanced surface catalytic activity [8, 9].

Despite extensive research on ferrites such as $ZnFe_2O_4$, $CoFe_2O_4$, and $NiFe_2O_4$, the gas sensing potential of tin ferrite ($SnFe_2O_4$) has been relatively underexplored [9]. $SnFe_2O_4$ presents a unique combination of Sn and Fe cations with variable oxidation states, potentially enhancing surface reactivity and gas adsorption. Various synthesis techniques-such as co-precipitation, sol-gel, combustion, and solid-state reactions-have been employed to fabricate $SnFe_2O_4$ nanomaterials [10, 11]. Among these, the hydrothermal method offers significant advantages, including better control over particle size, morphology, and crystallinity under relatively mild conditions [12], making it a highly suitable approach for preparing functional metal oxide nanostructures for gas sensing.

In this work, we report the hydrothermal synthesis of $SnFe_2O_4$ nanomaterials and a systematic investigation of H_2 gas sensing properties of $SnFe_2O_4$. A series of samples were prepared at varying hydrothermal temperatures to examine the impact of synthesis conditions on their microstructural characteristics and sensing performance. The sample synthesized at 200°C exhibited the most favorable response behavior, highlighting the crucial role of synthesis temperature in optimizing sensor functionality. These results offer valuable insights into the structure–property relationships of $SnFe_2O_4$ and provide a solid foundation for further development of high-performance gas sensors based on spinel-type nanomaterials.

2. Experimental

2.1. Synthesis of $SnFe_2O_4$

All chemical reagents were of analytical grade and used without further purification. The starting materials included tin (II) chloride dihydrate ($SnCl_2{\cdot}2H_2O$), iron (III) chloride hexahydrate ($FeCl_3{\cdot}6H_2O$), sodium hydroxide (NaOH), ethanol (C_2H_5OH), and acetone (C_3H_6O). $SnFe_2O_4$ (SFO) nanomaterials were prepared via a hydrothermal process, as illustrated in Fig. 1A. Briefly, 0.722 g of $SnCl_2{\cdot}2H_2O$ (3.2 mmol) and 1.728 g of $FeCl_3{\cdot}6H_2O$ (6.4 mmol) were dissolved in 60 mL of deionized water under continuous magnetic stirring for 30 min, yielding a reddish solution due to the presence of Fe^{3+} ions. Separately, 2.72 g of NaOH was dissolved in 20 mL of deionized water and then added dropwise to the precursor solution under vigorous stirring for an additional 30 min. During this process, the solution gradually turned black, indicating precipitate formation. The resulting suspension was transferred into a 100 mL Teflon-lined stainless-steel autoclave and subjected to hydrothermal treatment

at different temperatures (180 °C, 200 °C, and 220 °C) for 24 h. After naturally cooling to room temperature, the precipitates were collected by filtration and washed repeatedly (5–6 cycles) with deionized water until the filtrate reached a pH of ~ 7. The products were then dried in an oven at 80°C for 24 h. Finally, the dried powders were calcined in air at 500 °C for 2 h to transform the intermediate hydroxide phase $SnFeO(OH)_5$ into crystalline spinel $SnFe_2O_4$.

2.2. Characterization

The crystalline structure of samples was examined by X-ray diffraction (XRD, D2 Phaser, Bruker). The morphology and particle size were observed using Scanning Electron Microscopy (SEM, JCM-7000).

2.3. Fabrication of Gas Sensors

Gas sensors were fabricated using a thick-film deposition method, as shown in Fig. 1B. The $SnFe_2O_4$ powders were dispersed in N-vinylpyrrolidone (NVP) via ultrasonication to form a homogeneous suspension. A controlled volume of the suspension was drop-cast onto a pre-cleaned electrode substrate, followed by drying and heat treatment at 500 °C for 2 h to form a uniform sensing layer. This method ensured good adhesion and uniform coverage, both essential for stable and reproducible gas sensing performance.

2.4. Gas Sensing Measurements

The sensing characteristics were evaluated using a measurement system at ITIMS, Hanoi Univesity of Science and Technology. The sensor resistance was monitored in real time while alternating between air and the target gas at various concentrations and operating temperatures. Details of the gas sensing setup are provided in [13].

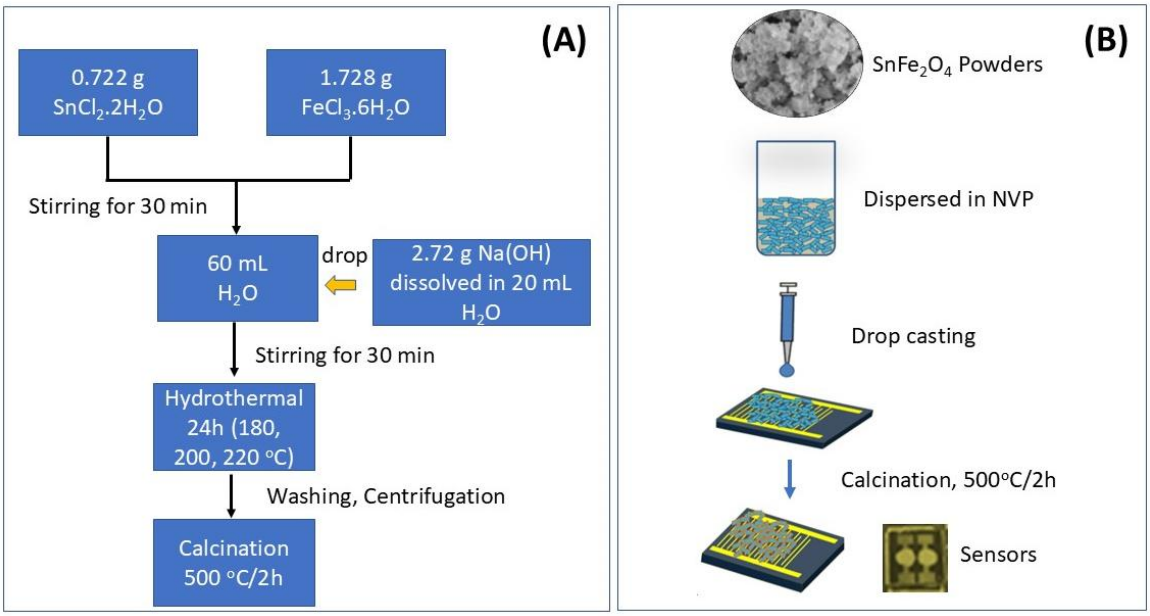

Figure 1. (A) Diagram of the hydrothermal synthesis of SFO, and (B) the gas sensor fabrication process.

3. Results and Discussion

The influence of hydrothermal temperature on the morphological evolution of $SnFe_2O_4$ particles is evident from the SEM observations. Fig.b2 presents SEM images of $SnFe_2O_4$ materials synthesized via the hydrothermal method at temperatures of 180 °C, 200 °C, and 220 °C. At 180 °C, the insufficient thermal energy leads to incomplete nucleation, resulting in irregular agglomerates and poorly defined particle boundaries. Increasing the temperature to 200 °C enhances both nucleation and growth processes, producing uniform spherical nanoparticles with an average size of approximately 100 nm. This indicates a balanced competition between nucleation and particle growth, favoring the formation of monodisperse structures. At the higher temperature of 220 °C, the system provides enough energy to promote oriented attachment and crystallographic alignment, giving rise to well-defined cubic morphologies. Such a transformation suggests that elevated temperatures facilitate the reorganization of primary nanoparticles into more thermodynamically stable spinel structures. Therefore, the hydrothermal temperature acts as a critical parameter in tuning particle shape and size, enabling controlled design of nanomaterials with tailored properties for gas-sensing applications.

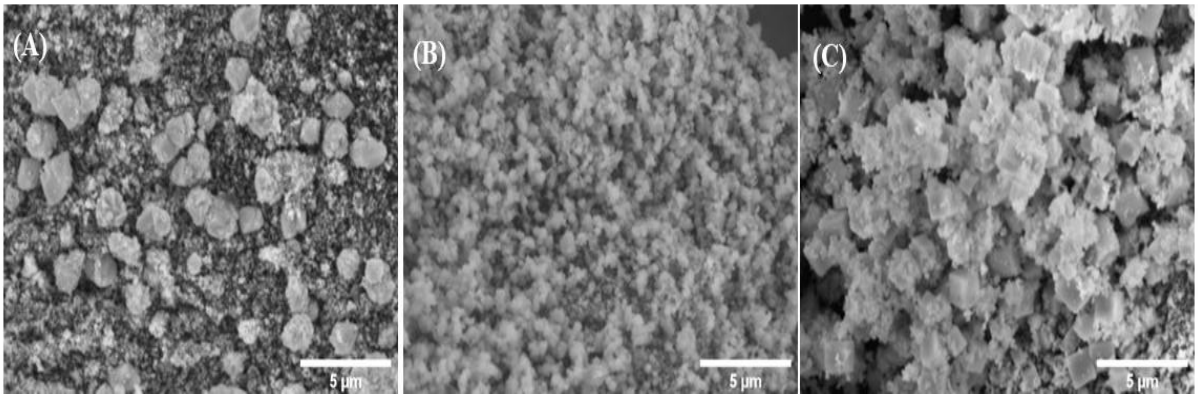

Figure 2. SEM images of the SFO samples synthesized at hydrothermal temperatures of (A) 180 °C, (B) 200 °C, and (C) 220 °C.

The XRD patterns of the SFO samples before and after calcination at 500 °C are presented in Fig. 3. As shown in Fig. 3 (A), the XRD pattern of the as-hydrothermally synthesized sample exhibits distinct diffraction peaks at 2θ values of 20.16°, 23.34°, 33.24°, 35.18°, 37.30°, 39.19°, and 41.04°, corresponding to the (111), (200), (211), (220), (222), (310), and (400) crystalline planes, respectively. These peaks match well with the standard diffraction data for orthorhombic $SnFeO(OH)_5$ (JCPDS #96-100-1745), indicating that the hydrothermal synthesis at 200 °C leads to the formation of well-crystallized $SnFeO(OH)_5$. The sharp and intense peaks confirm a high degree of crystallinity and the absence of additional peaks suggests high phase purity of the as-prepared material. These results demonstrate that hydrothermal treatment at 200 °C is sufficient to promote nucleation and growth of $SnFeO(OH)_5$ crystals, but not yet high enough to induce transformation into the spinel $SnFe_2O_4$ phase. This confirms $SnFeO(OH)_5$ as an intermediate phase before calcination, providing a favorable starting point for the controlled formation of spinel $SnFe_2O_4$.

Fig. 3(B) shows the XRD patterns after calcination at 500 °C, where a clear phase transformation from $SnFeO(OH)_5$ to spinel $SnFe_2O_4$ is observed. The calcined samples exhibit well-defined diffraction peaks at 2θ values of 18.28°, 30.11°, 35.48°, 37.09°, 43.13°, 53.45°, 57.03°, 62.62°, and 74.09°, corresponding to the (111), (202), (131), (222), (040), (242), (151), (404), and (353) crystalline planes

of the spinel structure, respectively. These peaks are in excellent agreement with the standard pattern for spinel $SnFe_2O_4$ (JCPDS #96-100-1050), confirming the successful transformation of $SnFeO(OH)_5$ into phase-pure $SnFe_2O_4$ upon calcination. The sharpness and intensity of the peaks indicate high crystallinity, and the absence of residual peaks from $SnFeO(OH)_5$ or any secondary phases confirms the phase purity of the final product. The formation of crystalline, phase-pure $SnFe_2O_4$ with a spinel structure is critical for enhancing gas sensing performance due to its high density of active sites and improved structural stability.

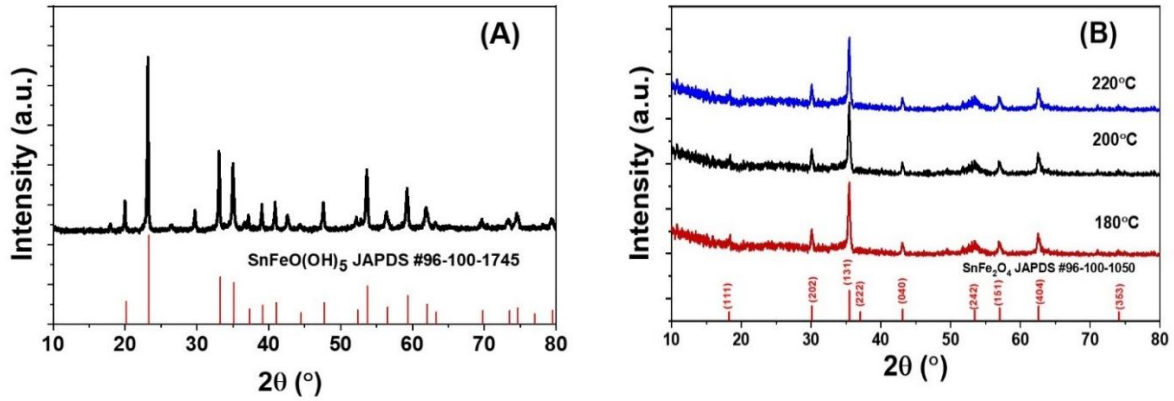

Figure 3. (A) XRD pattens of as-hydrothermal products, (B) XRD patterns of the SFO samples synthesized at hydrothermal temperatures of (a) 180 °C, (b) 200 °C, and (c) 220 °C.

Moreover, the XRD patterns of $SnFe_2O_4$ samples synthesized via hydrothermal treatment at 180 °C, 200 °C, and 220 °C show no significant differences in peak positions or relative intensities. All samples display diffraction peaks consistent with the spinel $SnFe_2O_4$ phase, indicating successful phase formation across the studied hydrothermal temperature range. The similarity in XRD patterns suggests that hydrothermal temperatures from 180 to 220 °C do not notably influence the crystallographic phase of $SnFe_2O_4$, although variations in morphology and particle size, as observed by SEM, may still occur.

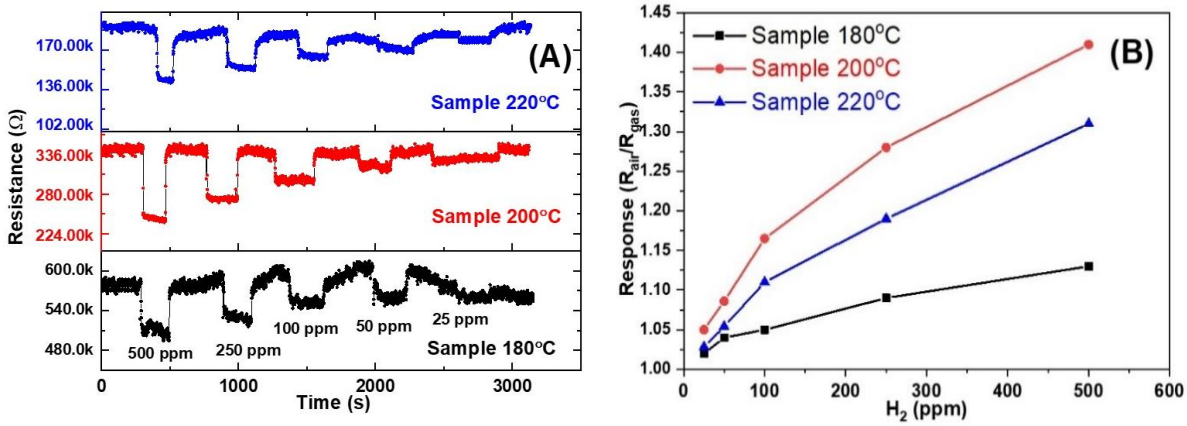

Figure 4. Gas sensing properties of the synthesized SFO samples: (A) Variation in resistance with H_2 concentration for samples synthesized at 180 °C, 200 °C, and 220 °C, measured at 400 °C; (B) Corresponding H_2 response of the samples.

Figs. 4 (A and B) illustrate the dynamic resistance response and corresponding sensitivity profiles of the $SnFe_2O_4$ sensors synthesized at 180 °C, 200 °C, and 220 °C, evaluated toward H_2 at an operating temperature of 400 °C. As observed in Fig. 4A), all sensors exhibit rapid, reversible, and stable changes in resistance upon exposure to H_2, reflecting their robust sensing capability. The decrease in resistance with increasing H_2 concentration unequivocally confirms the n-type semiconducting nature of $SnFe_2O_4$, wherein adsorption of reducing H_2 molecules enhances electron density in the conduction band, thereby lowering the resistance. Crucially, Fig. 4B demonstrates that the sensor synthesized at 200 °C achieves markedly superior response values compared to those prepared at 180 °C and 220 °C, especially at higher H_2 concentrations. This pronounced enhancement in sensing performance can be ascribed to the optimized microstructural features of the 200 °C sample, which likely balances high crystallinity with a favorable specific surface area, leading to an increased density of accessible and active adsorption sites for H_2 interaction. In contrast, the inferior response of the 180 °C sensor suggests incomplete crystallization and the presence of structural defects that can impede effective charge carrier modulation. Meanwhile, the moderate response of the 220 °C sample may stem from grain coarsening at higher hydrothermal temperatures, which reduces the surface-to-volume ratio and consequently limits the number of reactive sites. These results unequivocally underscore the critical role of hydrothermal synthesis temperature in tailoring the gas sensing properties of $SnFe_2O_4$ nanomaterials. The optimized synthesis at 200 °C yields a sensor with outstanding sensitivity and consistent response characteristics, positioning it as a promising candidate for high-performance hydrogen detection applications.

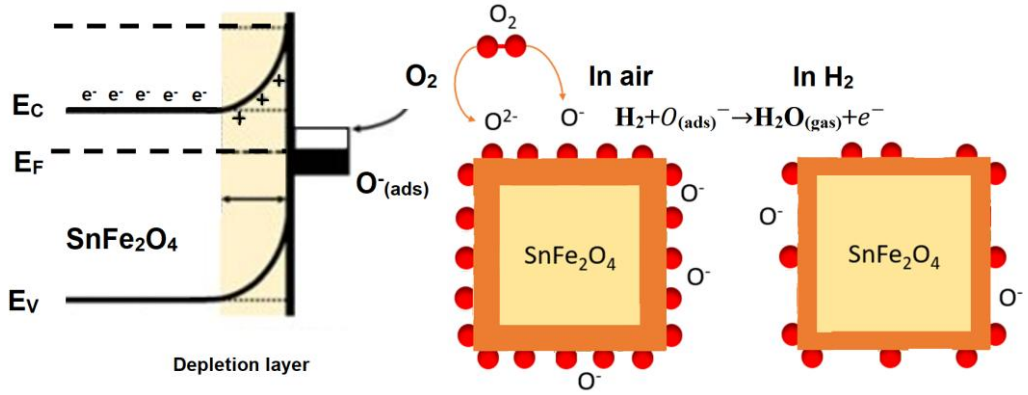

Figure 5. Electron depletion layer formation on $SnFe_2O_4$ surface in air and its modulation upon H_2 exposure.

The excellent H_2 sensing performance of $SnFe_2O_4$ can be rationalized by the classic depletion layer theory for n-type metal oxide semiconductors [14]. When the sensor is exposed to air at elevated temperatures (400 °C), oxygen molecules (O_2) are adsorbed onto the $SnFe_2O_4$ surface and capture electrons from the conduction band, forming chemisorbed oxygen species such as O^-, O_2^-, and O^{2-}. This process induces the formation of an electron depletion layer near the surface of $SnFe_2O_4$ particles, leading to a significant increase in the material's electrical resistance due to band bending and the formation of potential barriers at the grain boundaries (Fig. 5). Upon exposure to reducing gas H_2, the adsorbed H_2 molecules react with these chemisorbed oxygen species according to the reactions:

$$H_2+O_{(ads)}^- \rightarrow H_2O_{(gas)}+e^- \quad (1)$$

This reaction releases electrons back into the conduction band, effectively narrowing the depletion layer and lowering the potential barrier. Consequently, the electrical resistance of the sensor decreases sharply. The magnitude of resistance change is directly correlated with the concentration of H_2, as higher H_2 levels lead to more extensive reduction of chemisorbed oxygen and greater restoration of free carriers

[15]. The sensitivity of the sensor is thus highly dependent on the width and dynamics of the depletion layer: materials with higher surface area and appropriate crystallite size (as in the 200 °C sample) offer more active sites for oxygen adsorption and H_2 reaction, enhancing modulation of the depletion region and maximizing sensor response. Conversely, excessively large grains (as in the 220 °C sample) or poorly crystallized structures (as in the 180 °C sample) reduce the density or accessibility of active sites, leading to diminished sensing performance. Moreover, the spinel structure of $SnFe_2O_4$ provides abundant surface defect sites and promotes efficient adsorption–desorption kinetics, facilitating rapid and reversible sensor responses. This depletion layer-controlled mechanism underpins the high sensitivity, fast response, and reliable repeatability of $SnFe_2O_4$-based sensors for H_2 detection.

4. Conclusion

In this work, $SnFe_2O_4$ nanomaterials were successfully synthesized via hydrothermal approach at varying temperatures (namely 180 °C, 200 °C, and 220 °C), and their structural, morphological, and gas sensing characteristics were systematically evaluated. The obtained results clearly demonstrate that hydrothermal temperature plays a pivotal role in dictating both the morphological evolution and gas sensing performance of the resulting materials. Among the investigated samples, the sensor synthesized at 200 °C exhibited the largest response toward H_2 (25 to 500 ppm) at operating temperature of 400 °C. This is explained due to its highly uniform spherical nanoparticles (~100 nm) and optimized microstructural features. Microstructure analysis revealed that lower synthesis temperature (180 °C) led to irregular, poorly defined particles due to incomplete nucleation, while higher temperature (220 °C) facilitated the formation of cubic morphologies with signs of particle agglomeration, likely resulting in a reduced surface-to-volume ratio. The 200 °C-synthesized $SnFe_2O_4$ material thus achieves an ideal balance between crystallinity, particle size, and surface area, resulting in enhanced electron transport and gas-solid interactions. This work underscores the critical influence of synthesis parameters on the physicochemical and functional properties of spinel-type metal oxides and provides a rational design strategy for engineering high-performance hydrogen sensors based on $SnFe_2O_4$ nanostructures.

Acknowledgments

This research is funded by the Ministry of Science and Technology of Vietnam under Grant No. ĐTĐL.CN-35/23.

References

[1] T. T. Nguyet, L. Van Duy, N.C. Nam, D. Q. Dat, H. Nguyen, C.M. Hung, N. V. Duy, N. D. Hoa, Transition from p-type to n-type Semiconductor in V_2O_5 Nanowire-based Gas Sensors: Synthesis and Understanding of the Sensing Mechanism, Sensors Actuators B Chem., Vol. 424, No. 1, 2025, pp. 136841-136852, http://doi.org/10.1016/j.snb.2024.136841.

[2] M. Hjiri, N. Benmansour, F. M. Barakat, G. Neri, Metal Oxide Gas Sensors with Nanosheet Morphology: A review, Microchem. J., Vol. 215, No. 6, 2025, pp. 114510-114522, http://doi.org/10.1016/j.microc.2025.114510.

[3] L. Miranda, C. Duc, N. Redon, J. Pinheiro, B. Dorizzi, J. Montalvao, M. Verriele, J. Boudy, Automatic Detection of Indoor Air Pollution-related Activities using Metal-oxide Gas Sensors and the Temporal Intrinsic Dimensionality Estimation of Data, Indoor Environ., Vol. 1, No. 3, 2024, pp. 100026-100037, http://doi.org/10.1016/j.indenv.2024.100026.

[4] S. Yu, X. Jia, J. Zhang, W. Yang, H. Song, Recent Advances in Different Materials for Moisture Resistance of Metal Oxide-based Gas Sensors: A Review, Chem. Eng. J., Vol. 505, No. 2, 2025, pp. 159639-159654, http://doi.org/10.1016/j.cej.2025.159639.

[5] A. Afzal, β-Ga_2O_3 Nanowires and Thin Films for Metal Oxide Semiconductor Gas Sensors: Sensing Mechanisms and Performance Enhancement Strategies, J. Mater., Vol. 5, No. 4, 2019, pp. 542-557, http://doi.org/10.1016/j.jmat.2019.08.003.

[6] N. Van Hoang, C. M. Hung, N. D. Hoa, N. V. Duy, N. V. Hieu, Facile on-chip Electrospinning of $ZnFe_2O_4$ Nanofiber Sensors with Excellent Sensing Performance to H_2S Down ppb Level, J. Hazard. Mater., Vol. 360, No. 6, 2018, pp. 6-16, http://doi.org/10.1016/j.jhazmat.2018.07.084.

[7] N. H. Hanh, L. V. Duy, C. M. Hung, C. T. Xuan, N. V. Duy, N. D. Hoa, High-Performance Acetone Gas Sensor Based on Pt-Zn_2SnO_4 Hollow Octahedra for Diabetic Diagnosis, J. Alloys Compd., Vol. 886, 2021, pp. 161284-161295, http://doi.org/10.1016/j.jallcom.2021.161284.

[8] Q. Luo, Y. Wan, Z. Wang, S. Gao, Y. Chen, C. Feng, Excellent-Performing Gas Sensor based on Yttrium-Doped $ZnFe_2O_4$ Nanofibers for Detection of n-Butanol, J. Alloys Compd., Vol. 1027, No. 3, 2025, pp. 180605-180616, http://doi.org/10.1016/j.jallcom.2025.180605.

[9] Z. Zheng, K. Liu, Y. Zhou, Z. Zhang, H. Su, X. Nie, M. Debliquy, Z. Yu, C. Zhang, Spinel Type MCo_2O_4 (M = Mn, Mg, Ni, Cu, Fe and Zn) for Chemoresistance Gas Sensors, Mater. Today Chem., Vol. 36, No. 112023, 2024, http://doi.org/10.1016/j.mtchem.2024.101928.

[10] H. Han, Y. Luo, Y. Jia, N. Hasan, C. Liu, A Review on $SnFe_2O_4$ and their Composites: Synthesis, Properties, and Emerging Applications, Prog. Nat. Sci. Mater. Int., Vol. 32, No. 5, 2022, pp. 517-527, http://doi.org/10.1016/j.pnsc.2022.09.005.

[11] F. C. Zhou, Y. H. Sun, S. Liu, J. M. Nan, Synthesis of $SnFe_2O_4$ as a Novel Anode Material for Lithium-ion Batteries, Solid State Ionics, Vol. 296, 2016, pp. 163-167, http://doi.org/10.1016/j.ssi.2016.09.019.

[12] M. Ashan, H. A. Alyousef, A.W. Alrowaily, B. M. Alotaibi, N. A. Harbi, H. H. Somaily, M. Aslam, K. Ahmad, S. Aman, Maximizing the Electrochemical efficiency of Ce Doped $SnFe_2O_4$ through Hydrothermal Route for Supercapacitor Applications, Electrochim. Acta, Vol. 504, No. 7, 2024, pp. 144840-144852, http://doi.org/10.1016/j.electacta.2024.144840.

[13] L. V. Thong, L. T. N. Loan, N. V. Hieu, Comparative Study of Gas Sensor Performance of SnO_2 Nanowires and their Hierarchical Nanostructures, Sensors Actuators, B Chem., Vol. 150, No. 1, 2010, pp. 112-119, http://doi.org/10.1016/j.snb.2010.07.033.

[14] V. T. Duoc, H. Nguyen, T. M. Ngoc, C. T. Xuan, C. M. Hung, N. V. Duy, N. D. Hoa, Hydrogen Gas Sensor based on Self-heating Effect of SnO_2/Pt Thin Film with Ultralow Power Consumption, Int. J. Hydrogen Energy, Vol. 61, No. 3, 2024, pp. 774-782, http://doi.org/10.1016/j.ijhydene.2024.02.180.

[15] P. Ghosh, A. Mukherjee, M. Fu, S. Chattopadhyay, P. Mitra, Influence of Particle Size on H_2 and H_2S Sensing Characteristics of Nanocrystalline Nickel Ferrite, Phys. E Low-Dimensional Syst. Nanostructures, Vol. 74, 2015, pp. 570-575, http://doi.org/10.1016/j.physe.2015.08.023.